INTERNATIONAL JOURNAL OF ADVANCED STUDIES
IN COMPUTER SCIENCE AND ENGINEERING
IJASCSE VOLUME 11 ISSUE 4

04/30/2022

Composites Active Material for Detection of Faults in the Asynchronous Motor

Amar REGAZ[1], Larbi BOUKEZZI[1], Boubakeur ZEGNINI[2], Djellali MAHI[2]

[1]*Materials Science and Informatics Laboratory, MSIL, Ziane Achour University of Djelfa*
PO Box 3117 Road Moudjbara, 17000 Djelfa, Algeria
e-mail: a_regaz@yahoo.fr, larbiboukezzi@gmail.com

[2]*Studies and Development of Semiconductor and Dielectric Materials Laboratory, LeDMaScD*
Amar Telidji university of Lagouat
e-mails: b.zegnini@lagh-univ.dz, d.mahi@lagh-univ.dz

Abstract— **In this work, we detected the defects of the asynchronous electric machine under normal conditions and without load by installing multi-layer sensor active materials at the stator (Terfenol-D and PZT-5H). The magnetic field in the stator deforms the magnetostrictive layers and this distortion in turn affects the piezoelectric layer, which leads to the polarization of this layer and the appearance of a potential difference between their terminals. We chose the finite element method for the numerical solution. This method is a more powerful and versatile numerical technique for handling problems involving complex geometries and inhomogeneous media.**

Keywords— **Piezoelectric, Magnetostrictive, BRB defects diagnosis, asynchronous machine.**

I. Introduction

For the modeling of piezoelectric active materials, we returned to our work [1]-[3] where we modeled these materials in the static regime and the frequency regime, for the magnetostrictive materials we returned to our work [4], where we also modeled these materials at the frequency regime also the work of K. Azoum and all[5], and Claeyssen F[9].

The work of [10] used an electrical circuit model. In this model, the currents in the broken bar are canceled and the flow currents in the adjacent bars are increased. However, these bars can be only degraded but not completely broken and this state can be modeled with a low electrical conductivity of the corresponding bar [11] or by a high resistance in which increases the resistance of the rotor bar [10]. Secondly, they are definitely broken by zero electrical conductivity [11]. We also defined the breaking of the bars in the rotor on the basis that the electrical conductivity is zero [11].

We are using magnetostrictive material Terfenol-D, whoever is capable of providing a positive magneto-strain of a typical range of 800-2000 *ppm* at 50-200 kA/m in bulk materials [12] and about 4000 *ppm* at mechanical resonance frequencies and at high magnetic fields [13] [14].

We have installed a piezoelectric layer in the stator to detect stator faults[1]. The result that we acquired was satisfactory but in the case of detection of broken of the bars in the rotor, we could not, because the difference of potential obtained is very low, so we installed a sensor in the rotor, which led to the problem of recovering the potential difference across (collector brooms), This is the reason why we first excluded the magnetostriction phenomenon in the rotor and the stator and replaced it with two layers of giant magnetostrictive material in order to obtain a large deformation, then separated by a piezoelectric layer in order to obtain a measurable potential.

The magnetic field in the stator deforms the magnetostrictive layers, and in turn deforms the piezoelectric layer, resulting in the creation of a potential difference between the two ends thereof. By comparing these results with those in which the machine is healthy, we can determine the fault, whether it was cut at the stator or broken bars at the rotor. In addition, this technique makes it possible to obtain the potential difference directly between the ends of the sensor, unlike the technique which consists in measuring the magnetic field in air gap and then processing the signal[15]-[17], which takes time.

II. The System Components (Machine and Sensor)

Our system consists of an asynchronous electric machine equipped with a sensor as shown in Figure (1), The machine consists mainly of FerSi3% (stator and rotor) and copper (36 notches carry electrical conductors in the stator), as well as aluminum (28 aluminum bars at the rotor) and air separates the stator and the rotor. The sensor consists mainly of two

layers of giant magnetostrictive material (Terfenol-D) separated by a layer of piezoelectric material (PZT-5H).

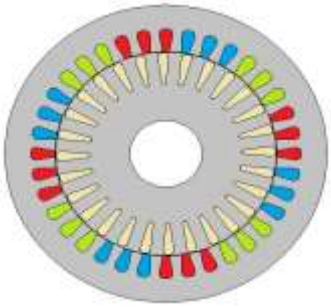

Fig.1. Geometry of asynchronous machine

III. LAWS OF BEHAVIOUR

Since the rotor and the stator of the electric machines are often made of iron alloy such as the iron FerSi3% their relative elongation is maximum of 60 *ppm*, we excluded this elongation and replaced by the elongation of two layers of materials having a considerable elongation up to 2000 *ppm* [18] [19], for this reason the magnetic phenomena remain at the stator and the rotor only:

$$B = \mu_0 \mu_r H \tag{1}$$

With:

B: magnetic induction, H: magnetic field, μ_0: permeability of a vacuum and μ_r: relative permeability.

With regard to the copper, vacuum and aluminum bars, the magnetic induction is proportional to the magnetic field:

$$B = \mu_0 H \tag{2}$$

Aluminum rods cause an induced electric current:

$$J_{ind} = \delta E \tag{3}$$

With:

J_{ind}: induced electric currents, E: electric filed and δ: electrical conductivity.

The sensor consists of Terfenol-D. This material is the place of coupling of magnetic phenomena and mechanical phenomena. It is mainly about the coupling between the magnetic induction and the deformation and we express it by the following system equations [20] [21]:

$$\begin{aligned} \{\varepsilon\} &= [S^H]\{\sigma\} + [d]\{H\} \\ \{B\} &= [d]^T\{\sigma\} + [\mu^\sigma]\{H\} \end{aligned} \tag{4}$$

With:

ε: strain, σ: stress, H: magnetic field and B: magnetic induction.

μ^σ: magnetic permeability tensor of material under a constant mechanical stress.

S^H: mechanical elasticity tensor under a constant magnetic field.

d: magneto-mechanical coupling tensor under a stress and a given magnetic field.

The ceramic PZT-5H which is the place of coupling between electrical phenomena and mechanical phenomena. It is mainly about the coupling between the electric induction and the deformation and we express it by the following system equations [22] [23]:

$$\begin{aligned} \{\varepsilon\} &= [S^E]\{\sigma\} + [e]\{E\} \\ \{D\} &= [e]^T\{\sigma\} + [\xi^\sigma]\{E\} \end{aligned} \tag{5}$$

With:

ε: strain, σ: stress, E: electric field and D: electrical induction.

S^E: tensor of mechanical elasticity under a constant electric field.

ξ^σ: tensor of electrical permittivity of material under a constant mechanical stress.

e: Electro-mechanical coupling tensor under a stress and a given electric field.

IV. FINITE ELEMENTS FORMULATION

A. PDE for piezoelectric material

The elastic behaviour en equilibrium and Gauss Law of the solid are described by following system equations:

$$e\nabla \bullet \nabla U - \xi^\sigma \nabla^2 V = 0 \tag{6}$$

$$\rho\omega^2 U + \nabla \bullet s^E \nabla U + e^t \nabla^2 V = 0 \tag{7}$$

With:

V: Electric potential.

After the discretization and the assembly we can write the system of algebraic equation as follows:

$$\begin{bmatrix} [K^\xi] & [K^e] \\ [K^e]^t & [K^s] - \rho\omega^2 [M^\rho] \end{bmatrix} \begin{Bmatrix} V \\ U \end{Bmatrix} = \begin{Bmatrix} 0 \\ 0 \end{Bmatrix} \tag{8}$$

B. PDE for magnetostrictf material

For piezoelectric material the elastic behaviour en equilibrium and Ampere Law of the solid are described by following system equations:

$$jo\omega A + \nabla \times \frac{1}{\mu^{\sigma}}\left(\nabla \times A - d^{'} s^{H^{-1}} \varepsilon\right) = J_{ext} \quad (9)$$

$$\rho\omega^2 U + \nabla \bullet \frac{1}{s^{'H}}\left(\varepsilon - \frac{d}{\mu^{\sigma}} B\right) = 0 \quad (10)$$

With:

A: Magnetic vector potential, J_{ext}: external current density, and U: displacement vector.

After the discretization and the assembly, we can write the algebraic equation system as follows:

$$\begin{bmatrix} [K^{\mu}] & [K^{d}] \\ [K^{d}] & [K^{s}] - \rho\omega^2 [M^{\rho}] \end{bmatrix} \begin{Bmatrix} A \\ U \end{Bmatrix} = \begin{Bmatrix} J_{ext} \\ 0 \end{Bmatrix} \quad (11)$$

C. Numerical modeling

We have developed a computation program under the Matlab environment capable of solving a system of equations in the following form:

$$d_a \frac{\partial^2 U}{\partial t^2} - \nabla . C_{ijkl} \nabla U + aU = f_i \quad (12)$$

With:

d_a: mass coefficient, C_{ijkl} : diffusion coefficient, a_{ij} : absorption coefficient and f_i : source term.

For the 2D piezoelectric system described above, the general solution vector is:

$$U = \begin{pmatrix} V \\ u \\ v \end{pmatrix} \quad (13)$$

Where:

V: Electric potential, u: displacement component along the x-axis and v is displacement component along with the y-axis.

For the 2D magnetostrictif system described above, also the general solution vector is:

$$U = \begin{pmatrix} A \\ u \\ v \end{pmatrix} \quad (14)$$

Where:

A: Magnetic vector potential, u: displacement component along the x-axis and v is displacement component along with the y-axis.

Each of the coefficients: d_a, C_{ijkl}, a_{ij} and f_i from equation (12) depends on the laws of behaviour in the studied region; we can synthesize them in the following table (1):

TABLE I
COEFFICIENTS OF THE SYSTEM EQUATIONS (12) [02] [03]

coefficients	**stator and rotor**	**copper (Electric conductor)**	**Aluminum (rotor bars)**	**Air-gab**
d_a	*0*	*0*	$-\delta\omega^2$	*0*
C_{ijkl}	$\mu_0\mu_r$	μ_0	μ_0	μ_0
f_i	*0*	$J_{ext}sin(\omega t)$ $J_{ext}sin(\omega t+2\pi/3)$ $J_{ext}sin(\omega t-2\pi/3)$	*0*	*0*

	Terfenol-D	**PZT-5H**
d_a	$-\rho_t\omega^2$	$-\rho_p\omega^2$
C_{ijkl}	$\begin{bmatrix} [K^{\mu}] & [K^{d}] \\ [K^{d}]^T & [K^{s}] \end{bmatrix}$	$\begin{bmatrix} [K^{\xi}] & [K^{e}] \\ [K^{e}]^T & [K^{s}] \end{bmatrix}$
f_i	0	0

Where:

$[K^{\mu}]$ is the magnetic stiffness matrix and is defined by the following relation:

$$[K^{\mu}] = -\int_v [B_w][\mu^{\sigma}][B_w] dv \quad (15)$$

$[K^S]$ is the mechanical rigidity matrix and is defined by the following relation:

$$[K^s] = \int_v [B_u][s^H][B_u] dv \quad (16)$$

$[K^d]$ is stiffness magneto-mechanical coupling matrix given by

$$[K^d] = \int_v [B_u][d][B_w] dv \quad (17)$$

$[K^{\xi}]$ is the matrix of electrical stiffness and is defined by the following relation:

$$[K^{\varepsilon}] = -\int_v [B_w]^t [\varepsilon'^{\sigma}][B_w] dv \quad (18)$$

$[K^e]$ is electromechanical coupling matrix given by:

$$[K^e] = \int_v [B_u]^t [e][B_w] dv \quad (19)$$

D. Boundary conditions:

The boundary conditions of the external electric machine are Dirichlet, and the boundary conditions of the sensor are illustrated in Figure (2):

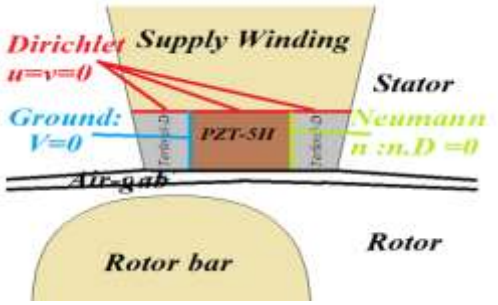

Fig.2. Boundary conditions in the sensor

V. Results and Discussions

Initially, you should take a look at the magnetic card of our three-phase asynchronous machine that has four poles. Figure (3.a) shows the equipotential lines of the electric potential A_z and shows that these lines close and create four alternating poles. Figure (3.b) shows the magnetic flux density distribution in the machine is shown that under these operating conditions the machine is not saturated.

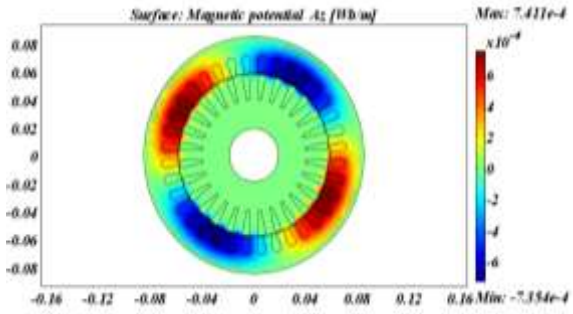

(a)

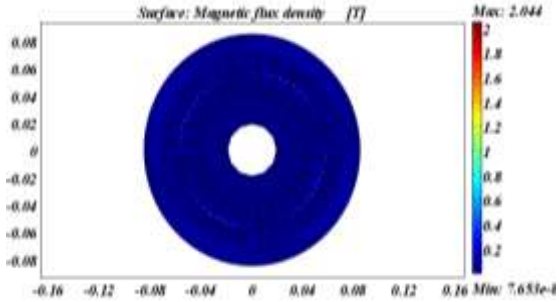

(b)

Fig.3. Distribution in the machine: (a) Magnetic potential A_z(b) Magnetic flux density

We will study two possible configurations to have a well amplified electric potential, the first is for a sensor in a horizontal position and the other for a sensor in a vertical position to arrive at the best fault detection configuration.

A. Horizontal configuration

We chose the location of the sensor in light of the previous study in which we found that it was best positioned as shown in Figure (3), which also represents the total displacement of the sensor.

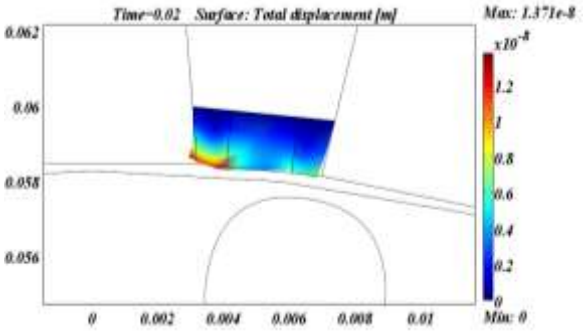

Fig.3. Total displacement in the sensor

Figure (4.a and b) show the displacement component u along the x-axis and the displacement v along the y-axis respectively allow choosing the material polarization. It is clear that u is greater than v so we must polarize our materials along the ox axis consequently the coupling matrix of piezoelectric material will be:

$$\begin{bmatrix} 0 & 0 & d_{22} \\ d_{12} & d_{12} & 0 \end{bmatrix}$$

Where d_{12} and d_{22} are the electromechanical coupling coefficients.

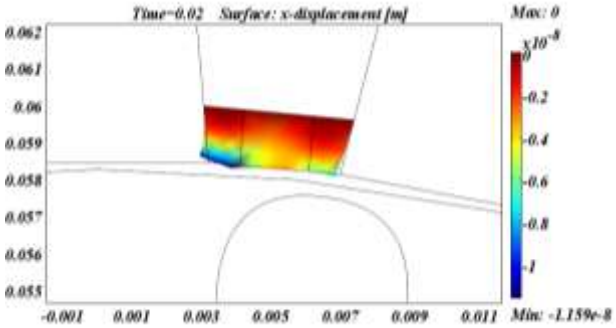

(a)

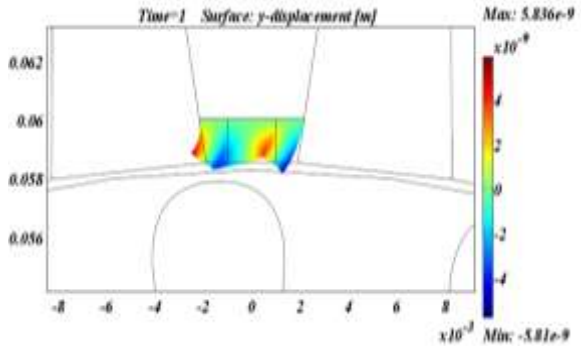

(b)

Fig.4. Displacement in the sensor: (a) vertical displacement (b) horizontal displacement.

Figure (5) shows the distribution of the electrical potential obtained to the ceramic material PZT-5H which reaches 0.92 *mvolts*. Figure (6) shows the variation of this potential produced between their electrodes as a function of time when the machine is healthy.

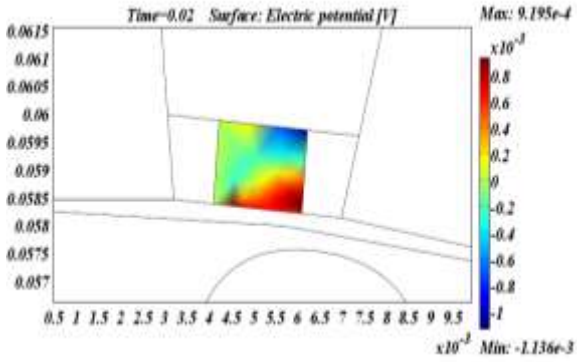

Fig.5 Distribution of the electrical potential

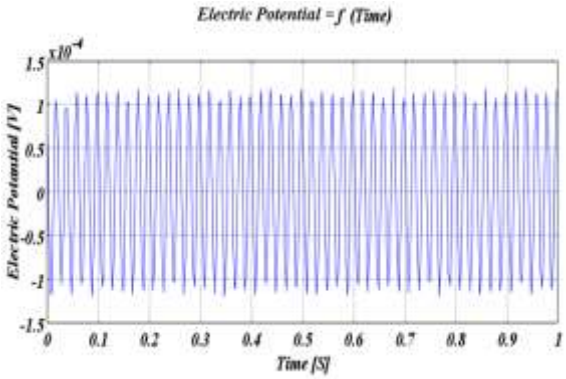

Fig.6 Potential produced between their electrodes of sensor as a function of time when the machine is healthy

Figure.7. shows a comparison of the potential differences in the case of a supply phase broken down with the potential difference when the machine is healthy. We note here a decrease of this potential, which explains that the energy given to the machine decreases when a phase breaks and thus decreases the electrical potential between the electrodes of the sensor [01], while the Figure (8) clearly shows what we said about the potential decrease between the sensor electrodes when two phases break at the same time.

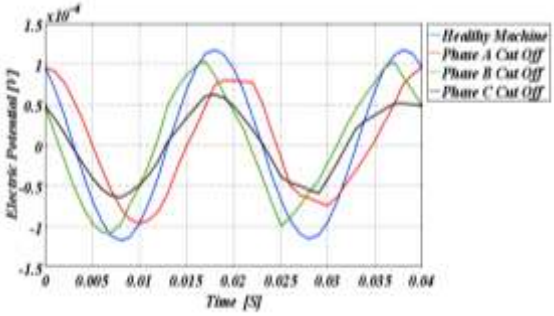

Fig.7 Voltages created in the sensors with the different cuts of the phases

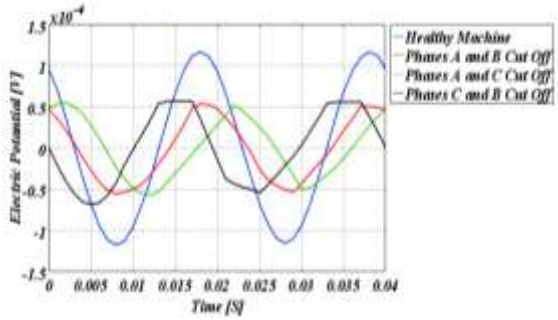

Fig.8 Voltages created in the sensors with the different cuts of the two phases

Figure (9) shows that the comparison of the potential difference produced in the case of the machine is healthy with the potential obtained in the case of a broken bar in the rotor, two non-adjacent bars and two adjacent bars. We clearly note that the significant potential difference of 0.15 *mvolts* even though the sensor is installed in the stator.

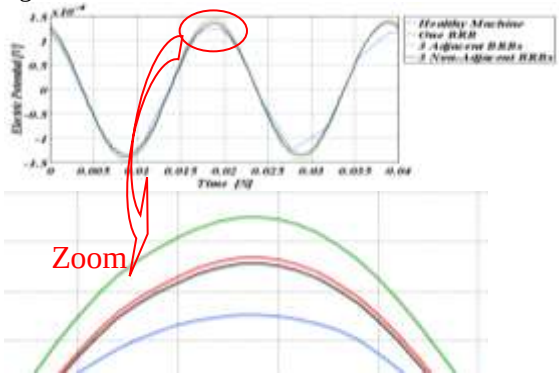

Fig.9 Voltage created in the sensors with the different BRBs

B. Vertical configuration

This configuration is illustrated in Figure (10) that is layer of piezoelectric material between two transverse magnetostrictive layers.

this second configuration allows us to increase the total displacement expected almost five times higher than the previous configuration as shown in Figure (11), the U and V displacements allow us to choose the polarization of our materials and as in the previous case we choose it according to the axis which has a higher displacement, in this case, the chosen axis is the axis of the x-axis as shown in Figure (12).

This last configuration also allows us to increase the potential value generated in the piezoelectric material up to nearly four times compared to the previous potential as shown in Figure.13.

We notice that there is a decrease in potential when there is a phase cut off as shown in Figure (14) or two phases cut off at the same time as shown in Figure (15) and all these quantities larger than in the previous configuration.

In the end, we look forward to detecting broken rotor bars better than the previous configuration and it is illustrated by the Figure (16).

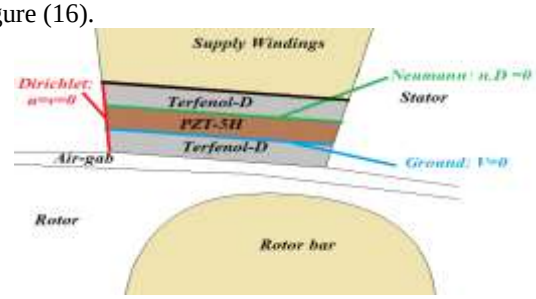

Fig.10. Boundary conditions in the sensor

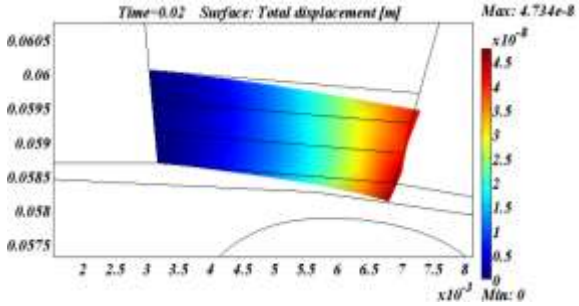

Fig.11. Total displacement in the sensor

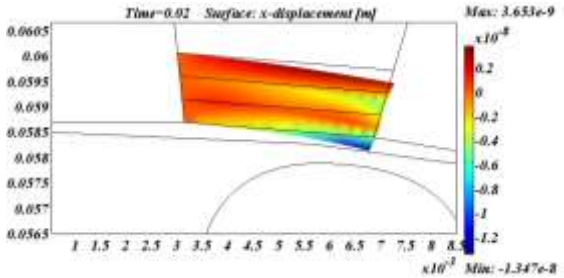

(a)

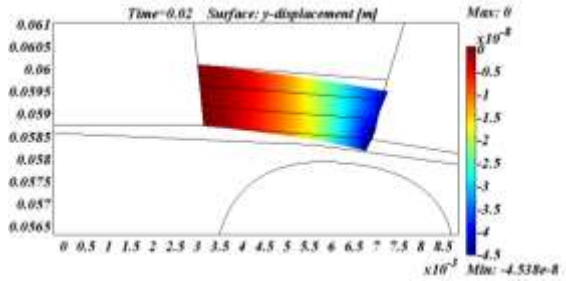

(b)

Fig.12. Displacement in the sensor: (a) vertical displacement (b) horizontal displacement.

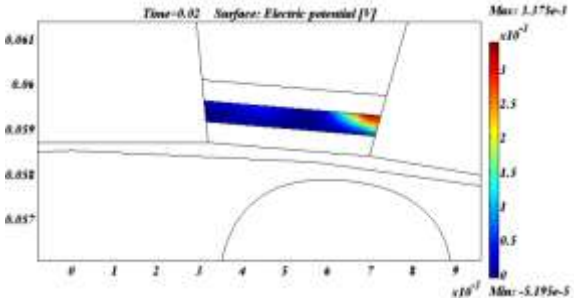

Fig.13 Distribution of the electrical potential

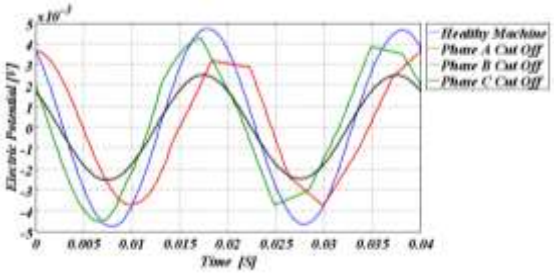

Fig.14 Voltages created in the sensors with the different cuts of the phases

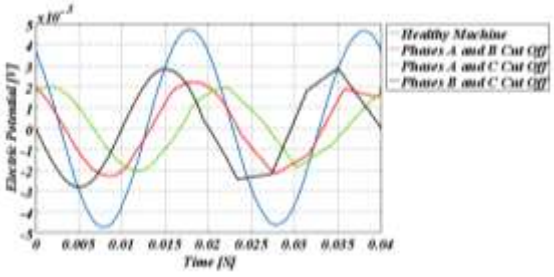

Fig.15 Voltages created in the sensors with the different cuts of the two phases

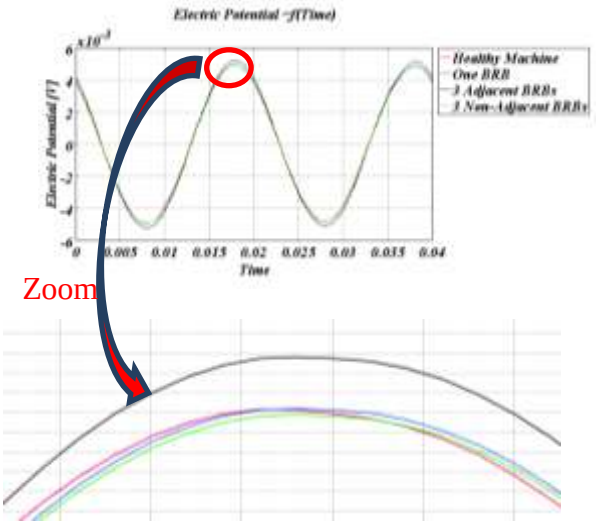

Fig.16 Voltage created in the sensors with the different BRBs

VI. Conclusion

In this paper, we have proposed the use of a multilayer sensor of active materials, which allowed amplifying the resulting electric potential, and also allowed us to detect rotor failures and exclude the sensor in the rotor to detect them. We additionally compared the results obtained with results where the machine is healthy in order to determine the phase breaks in the stator or broken of the bars in the rotor.

VII. Future scope

In the future, we aspire to take into account the saturation of the motor because in this case the magnetic reluctivity and the relative displacement will change according to the applied field, therefore we have a non-linear relationship between the inductance and the magnetic field in the motor carcass on the one hand and on the other we have a non-linear relationship between relative displacement and constraint. Which will definitely reflect positively on the results obtained.

Acknowledgment

This research project was supported by Ministry of Higher Education and Scientific Research, People's Democratic Republic of Algeria. We are extremely thankful to the head of Laboratory of Materials Science and Informatics, Ziane Achour University of Djelfa, Algeria which helped us in successfully completing our project work. Also we would like to extend our sincere esteems to all staff in laboratory for their timely support .

References

[1] Regaz A, Zegnini B, Mahi D, Boukezzi L. Detection of faults in the asynchronous machine by the use of smart materials. *Diagnostyka*. 2018;19(3):43-54. https://doi.org/10.29354/diag/93230

[2] Regaz A, Zegnini B, Mahi D, Boukezzi L. Static and harmonic behavior of piezoelectric beam bending actuators. *Electrotechnica, Electronica, Automatica, (EEA)*, 2017; 65(4): 30-36.

[3] Regaz A, Boukezzi L, Zegnini B, Mahi D. Contribution to the study of piezoelectric beam bending actuator in harmonic mode. *5th International Conference on Electrical Engineering (ICEE-B)*, 2017:1-5.https://doi.org/10.1109/ICEE-B.2017.8192191

[4] Regaz A, Boukezzi L, Zegnini B, Mahi D. Contribution to the study of piezomagnetic materials. *4th International Conference on Electrical Engineering (ICEE-B)*, 2015: 1-4. https://doi.org/10.1109/INTEE.2015.7416833

[5] K. Azoum, M. Besbes M, F. Bouillaut, (2004). 3D FEM magnetostriction phenomena used coupled constitutive laws, *International Journal of Applied Electromagnetic and Mechanics*, no. 19, pp 367-371.

[6] T.T. Nguyen, (2011), Modeling with finite elements of magneto-electric composite materials, PhD thesis, University of Paris (2011) (in French).

[7] Benbouzid M.E.H., Body C., Reyne G., Meunier G., Finite Element modelling of giant magnetostriction in thin film, IEEE, *Trans. on Mag.*, vol. 31, no 6, p. 3563-3565, novembre 1995.

[8] Ludwing A., Quandt E., Giant magnetostrictive thin films for applications in microelectromechnical systems, *J. Appl. Phys*. vol. 87 no 9, p. 4691-4695, may 2000.

[9] Claeyssen F., Giant dynamic magnetostrain in rare earth- iron magnetostrictive materials , *IEEE Trans. MAG*. 27, no 6, p. 5343-5345, novembre 1991.

[10] Kaikaa MY, Hadjami M, Khezzar A. Effects of the simultaneous presence of static eccentricity and broken rotor bars on the stator current of induction machine. *IEEE Trans. Ind. Electron*, 2014; 61(6): 2942-2942.

[11] Boughrara K, Takorabet N, Ibtiouen R, Touhami O, Dubas F. Analytical analysis of cage rotor induction motors in healthy, defective, and broken bars conditions. *IEEE Trans. Magn*, 2015; 51(2): 1-17.https://doi.org/10.1109/TMAG.2014.2349480

[12] F. Claeyssen, N. Lhermet, R. Le Letty, P. Bouchiloux, Actuators, Transducers and Motors Based on Giant Magnetostrictive Materials, *Journal of Alloys and Component*, 1997, Vol. 258, pp. 61-73.

[13] M. G. Aston, A. G. I. Jenner, W. J. Metheringham, K. Prajapati, Controlled High Power Actuation Utilizing Terfenol-D, *Journal of Alloys and Compounds*, 1997, Vol. 258, pp. 97-100.

[14] F. Claeyssen In: H. Janocha, editor. *Adaptronics and smart structures*. Germany: Springer Verlag; 1999, ISBN 3-540-61484-2. pp. 124–143.

[15] A. SEGHIOUR, T. SEGHIER, B. ZEGNINI,G. GEORGOULAS, "Multi-Class Classification Approach for the Diagnosis of Broken Rotor Bars based on Air-Gap Magnetic Flux Density", *in Electrotehnica, Electronica, Automatica (EEA)*, 2017, vol. 65, no. 2, pp. 31-39, ISSN 1582-5175.

[16] AM. Silva, RJ. Povinelli, S. Member al,"Rotor bar fault monitoring method based on analysis of air-gap torques of induction motors". *IEEE Trans Industr Inf*, 2013, Vol 9, pp. 2274–2283

[17] Arkkio A., "Finite element analysis of cage induction motors fed by static frequency converters". *IEEE Trans Magn*,1990, Vol. 26, pp. 551–554. https://doi:10.1109/20.106376

[18] Ludwig A, Quandt E. Giant magnetostrictive thin films for applications in micro-electromechanical systems, *J. Appl. Phys*. vol. 87, no 9, p. 4691-4695, May 2000.

[19] Quandt E, Ludwig A. Giant magnetostrictive multilayers. *J. Appl. Phys*, vol. 85, no 8, p. 6232-6237, 1999.

[20] Srinivasa Rao K, Srinivas G, Srinivas-Prasad MVVK, Srinivas Y, Shudheer B, Venkateswar Rao A. Design and simulation of MEMS based piezoelectric shear actuated beam. American J. Mater. Sci, 2012; 2(6):179184.https://doi.org/10.5923/j.materials.20120206.04

[21] Smiyh, I.M., Griffiths, D.V. Programming the finite element method. Second Edition, University of Manchester, UK (1988)
[22] Pefort, V., Preumoont, A., Finite element modeling of piezoelectric structures. *Samtech User's Conference*, Paris, France (2001).
[23] Pefort, V.: Finite element modeling of piezoelectric active structures. PhD thesis, Free of Bruxelles University, Brussels, Belgium, (2001).